# Fast Encoding and Decoding for Implicit Video Representation

Hao Chen<sup>1</sup>, Saining Xie<sup>2</sup>, Ser-Nam Lim<sup>3</sup>, and Abhinav Shrivastava<sup>1</sup>

University of Maryland, College Park, USA
 New York University, USA
 University of Central Florida, USA
 haochen.umd@gmail.com

**Abstract.** Despite the abundant availability and content richness for video data, its high-dimensionality poses challenges for video research. Recent advancements have explored the implicit representation for videos using neural networks, demonstrating strong performance in applications such as video compression and enhancement. However, the prolonged encoding time remains a persistent challenge for video Implicit Neural Representations (INRs). In this paper, we focus on improving the speed of video encoding and decoding within implicit representations. We introduce two key components: NeRV-Enc, a transformer-based hypernetwork for fast encoding; and NeRV-Dec, a parallel decoder for efficient video loading. NeRV-Enc achieves an impressive speed-up of  $\mathbf{10^4} \times$  by eliminating gradient-based optimization. Meanwhile, NeRV-Dec simplifies video decoding, outperforming conventional codecs with a loading speed  $\mathbf{11} \times$  faster, and surpassing RAM loading with pre-decoded videos  $(\mathbf{2.5} \times$  faster while being  $\mathbf{65} \times$  smaller in size).

**Keywords:** Implicit video representation · efficient video coding

## 1 Introduction

Video research is a fundamental area in computer vision, owing to its rich visual content and widespread presence. However, the immense size of video data presents challenges, as video storage, loading, and processing demands are orders of magnitude larger than those for images. Recent research has explored the potential of representing high-dimensional video data as deep neural networks [5-7,21,27,29]. These representations are favored in applications like video compression (achieving up to  $1000 \times$  size reductions while maintaining good visual quality), and video enhancement [5,6,12,27]. Unlike pixel-wise Implicit Neural Representation (INR) methods that use MLP networks to model individual pixels, the NeRV series [5-7,21] employs convolution neural networks to generate entire frames, enhancing video encoding and decoding efficiency.

Despite the efficiency gains achieved by the NeRV series, training a neural network to overfit a given video using gradient-based optimization remains time-consuming. Since video encoding involves mapping input video to NeRV

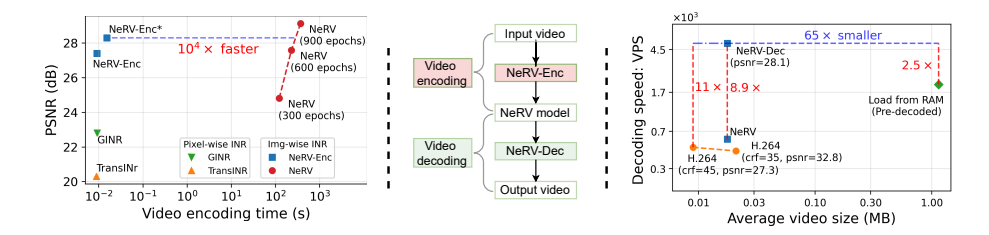


Fig. 1: Left: video encoding for implicit video representations. NeRV-Enc is  $10^4 \times$  faster than NeRV [6] baseline (with gradient-based optimization). \* uses a larger encoder and more training videos. Right: video decoding. NeRV-Dec decodes videos  $8.9 \times$  faster than NeRV and  $11 \times$  faster than H.264. It is even  $2.5 \times$  faster than loading pre-decoded videos from RAM while being  $65 \times$  smaller in video size.

model weights, we propose a straightforward alternative: NeRV-Enc. NeRV-Enc employs a hyper-network to directly generate model weights, thus avoiding the cumbersome encoding process. Our work addresses two fundamental questions: Can a hyper-network be effectively trained on a given video dataset? And can a well-trained hyper-network generalize well to unseen videos?

Given the outstanding performance of transformer networks in various visual tasks [4, 15, 22, 32, 49], we utilize transformers as the hyper-network. This hyper-network takes video patches and initial weight tokens as input, depicted in Fig. 2. Our research demonstrates that NeRV-Enc provides positive answers to the questions raised earlier. We show that it is indeed possible to train NeRV-Enc on training videos, and it effectively generalizes to unseen videos. In comparison to training NeRV with gradient-based optimization, NeRV-Enc significantly reduces the encoding time, achieving a speed-up of  $\mathbf{10^4} \times$  (Fig. 1 Left).

In addition to video encoding, efficient decoding plays a vital role. While a video is encoded just once, it can be decoded countless times. As such, the efficiency of decoding is critical for video playback, streaming, and preview. In the context of video research, especially in large-scale experiments, video loading involves a more complex decoding pipeline compared to image data loaders. Data loaders that require significant computational resources can prolong research cycles and present substantial hurdles when training video models with extensive datasets [51]. Indeed, data loading significantly hampers training efficiency, causing a slowdown of 46% in video self-supervised learning, as highlighted in [17]. In this context, video loading stands out as a critical bottleneck, hindering the progress of video research. To address this issue, we present NeRV-Dec, a parallel and efficient video loader based on NeRV.

Traditional video codecs, like H.264, face challenges with complex decoding pipelines, demanding customized design and optimization for specific applications. In contrast, our NeRV-Dec makes video decoding simpler and faster by efficient parallelization. As shown in Fig. 1 Right, NeRV-Dec is  $8.9\times$  faster than the NeRV baseline and achieves an  $11\times$  speed improvement over H.264. Notably, NeRV-Dec outperforms RAM loading of pre-decoded videos by  $2.5\times$  faster, while utilizing much less disk storage ( $65\times$  smaller). Unlike existing video codecs tai-

lored primarily for CPU use, NeRV-Dec emerges as the superior choice, especially in deep learning research. NeRV-Dec efficiently utilizes the power of advanced hardware like GPUs, TPUs, and NPUs, which are already the favored platforms for many users. It achieves this without the need for any specialized design or optimization for video loading, making it highly compatible and easy to integrate into existing workflows.

We outline the contributions of this paper as follows: **a)** We propose the NeRV-Enc architecture for obtaining image-wise implicit video representations (NeRV), achieving a  $10^4$  speedup in encoding compared to conventional gradient-based optimization methods. **b)** We extensively explore the architecture design of NeRV-Enc, addressing challenges in converting MLP to ConvNets and scaling up the training of NeRV-Enc. Specifically, we introduce layer-adaptive weight modulation for NeRV weights, which significantly outperforms previous modulation strategies in terms of efficiency. **c)** We introduce NeRV-Dec for parallel decoding of NeRV, achieving an  $8.9\times$  speedup over conventional NeRV decoding. NeRV-Dec also outpaces the common video codec H.264 by  $11\times$  in speed and is  $2.5\times$  faster than loading pre-decoded videos from RAM. **d)** Leveraging weight quantization, we reduce video size by  $65\times$  compared to the original.

#### 2 Related Work

Implicit Neural Representations. Recent advances in deep learning have given rise to implicit neural representations, which are compact data representations [6, 7, 16, 34]. These representations fit neural networks to signals like images, 3D shapes, and videos. A prominent subset of implicit representations is coordinate-based neural representations, which take pixel coordinates as input and produce corresponding values, such as density or RGB values, using MLP networks. These representations have demonstrated promise in diverse applications, including image reconstruction [42,48], image compression [16], continuous spatial super-resolution [2,8,23,45], shape regression [13,37], and novel view synthesis for 3D scenes [36,41].

In contrast to coordinate-based methods, NeRV [6] introduces an image-wise implicit representation that takes the frame index as input and outputs the entire frame without iterative pixel-wise computations. NeRV leverages convolutional neural networks, offering improved efficiency and regression quality compared to coordinate-based methods. By representing videos as neural networks, NeRV transforms video compression into model compression, achieving comparable performance with common video codecs through model pruning, quantization, and entropy encoding. Building on NeRV's success, works [5, 7, 21, 29] further enhance efficiency and shows superior performance in video compression, interpolation, and enhancement. Our approach leverages image-wise representations since NeRV series provide higher capacity and faster decoding speed compared to coordinate-based methods.

**Hyper-Networks.** Hyper-networks [19] are commonly employed to generate model weights for another neural network based on input data or a dataset. The

#### 4 Hao Chen et al.

concept of content-adaptive weights is prevalent in deep learning, exemplified in techniques like dynamic convolution [10] and conditional convolution [53]. Various methods have been developed to modulate model weights in a latent space [35, 37, 43, 44] rather than generating all weights directly, a strategy that can alleviate learning challenges. In these approaches, the neural network takes both pixel coordinates and a content-adaptive vector for modulation, where the modulated vectors serve as the hyper-networks. TransINR [9] and GINR [26] employ hyper-networks to generate model weights for pixel-wise INRs, suitable for image and video regression.

Efficient Video Codecs. Existing video dataloaders rely on traditional codecs like MPEG [28], H.264 [50], and HEVC [47] to reduce video size. Advanced video codecs like AV1 [11] and VVC [3] offer improved compression but at the expense of longer decoding times, hampering data loading speed. Recent developments in deep learning have introduced techniques for video compression, seeking to enhance traditional methods, including image compression, interpolation [14, 52], autoencoders [20], modeling conditional entropy between frames [31], and rethinking video compression with deep learning [1, 30, 40], or refine existing codecs [25, 39]. Although these learning-based methods improve bits-distortion performance, they introduce significant decoding latency, rendering them unsuitable for fast video loading.

In contrast, loading videos with implicit representations is straightforward, simple, and fast. NeRV [6], a recent implicit video representation, achieves comparable compression performance with traditional video codecs, by reshaping video compression into model compression. The video decoding process in NeRV is a simple feed-forward operation of the convolution network and can be seamlessly deployed across various devices without specific design or optimization. Drawing inspiration from NeRV, our NeRV-Dec significantly reduces video model size via quantization and entropy encoding. Meanwhile, it improves decoding speed further by enabling scalability and improved parallelization.

#### 3 Method

To improve the encoding speed of implicit video representation, we present NeRV-Enc. It employs a hyper-network denoted as  $g_{\phi}$  to generate weights  $\theta'$  for the NeRV model  $f_{\theta}$ , based on input video data  $x \in \mathbb{R}^{t \times 3 \times h \times w}$ . These learned weights are then used to reconstruct video frames, yielding  $\hat{x}_t = f_{\theta=\theta'}(t)$ . The primary objective is to minimize the reconstruction error between  $\hat{x}_t$  and the its ground truth  $x_t$  for training videos  $D_{\text{train}}$ , while ensuring the generalization to testing videos  $D_{\text{test}}$ . Additionally, we introduce NeRV-Dec, a method designed for parallel video decoding with good efficiency. Please consult Tab. 1 for a comprehensive list of symbol definitions.

#### 3.1 Video Encoding: NeRV-Enc

Generate Video-Specific Weights. We employ a Transformer network with L encoder layers as a hyper-network to generate video-specific model weights,

Variable	Definition
$\overline{x}$	Input video
$x_t$	Video frame at time $t$
$\hat{x}_t$	Reconstructed video frame at time $t$
$g_\phi$	Hyper-network (w/ parameter $\phi$ )
$f_{ heta}$	NeRV model (w/ parameter $\theta$ )
$ heta_0$	Initial weight tokens (hyper-network input)
$\hat{ heta}'$	Hyper-network output: video-specific weights
$ heta_1$	Video-agnostic model weights
heta'	Final NeRV model weights
$D_{\text{train}}, D_{\text{tes}}$	t Training and test set
$C_{\mathrm{out}}, C_{\mathrm{in}}$	Convolution output and input channel width
K, S	Kernel size, upscale factor for NeRV blocks
M	Number of video patches
N	Number of weight tokens
d	Token dimension for transformer encoder
$d_{ m out}$	Output dimension for weight tokens

Table 1: Variables and their definitions.

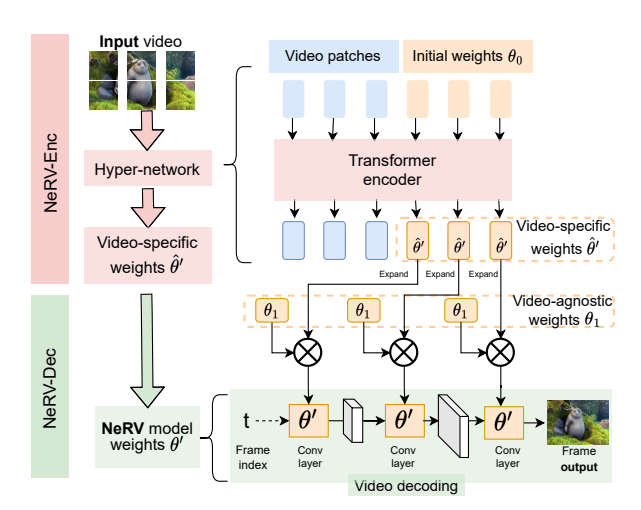


**Fig. 2:** Top: video encoding. NeRV-Enc processes the input video x to get video-specific weights  $\hat{\theta}'$  using the hyper-network. **Bottom:** video decoding. NeRV-Dec generates final NeRV weights  $\theta'$  and reconstruct video  $\hat{x}$ .

denoted as  $\hat{\theta}'$ . The input video x is partitioned into patches, which are then transformed into patch tokens using a fully connected (FC) layer. Additionally, learned position embeddings are added to these patch tokens. These patch tokens, in conjunction with the initial weight tokens  $\theta_0$ , form the input tokens. Subsequently, the hyper-network processes these input tokens to produce video-specific weights  $\hat{\theta}' \in \mathbb{R}^{d_{\text{out}} \times N}$ , which serves as an compact representation of the video. This encoding process is depicted in Fig. 2 Top and Fig. 4 Left.

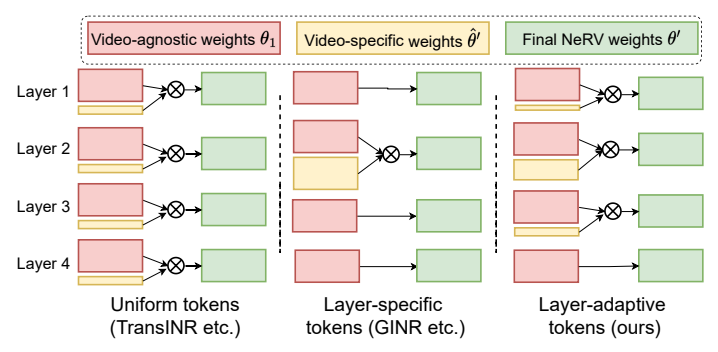


Fig. 3: Weight token distributions across layers. Left: Uniform (TransINR [9]). Middle: Layer-specific (GINR [27]). Right: Layer-adaptive (ours).

Adaptive Weight Tokens across Layers. We've observed that token importance varies across different layers. Unlike TransINR [9], which employs an identical number of weight tokens for all layers, or GINR [26], which restricts weight tokens to a specific layer (2nd layer), we introduce a flexible and adaptive approach to weight token distributions. This customization results in three distinct schemes: uniform weight tokens (TransINR), layer-specific weight tokens (GINR), and adaptive weight tokens (our approach), each designed to suit videospecific weight distribution across layers. These diverse weight distributions are visually depicted in Fig. 3.

NeRV-Enc for Video Restoration. Implicit video representations have proven to be good at video restoration tasks such as denoising and inpainting. Besides reconstruction, we also extend NeRV-Enc to various video restoration tasks. NeRV-Enc takes degraded videos as input and use ground truth videos as supervision. Evaluations on unseen videos indicate that NeRV-Enc effectively addresses these degradation tasks. Note that while previous implicit methods like NeRV and HNeRV demonstrate competence in restoration tasks, they often require additional supervision, such as masks for inpainting. Furthermore, their training might require reference data for the test video, like high-resolution or de-blurred frames. In contrast, NeRV-Enc leverages large-scale training to learn restoration capabilities and shows robust generalization to unseen videos. This makes NeRV-Enc a more practical and versatile tool for video restoration.

#### 3.2 Video Decoding: NeRV-Dec

Efficient Video Storage. Prior to video decoding, it is necessary to store the video-specific weights efficiently. To achieve storage efficiency, we employ weight quantization and entropy encoding for these weights, similar to compression techniques used in NeRV approaches [5,6].

Generate NeRV Weights. After obtaining the video-specific weights  $\hat{\theta}'$ , we move on to calculate the final weights  $\theta'$  for a NeRV model, which we represent as  $f_{\theta=\theta'}$ . As shown in Fig. 4 (b), the video-specific weights  $\hat{\theta}' \in R^{d_{\text{out}} \times N}$  for

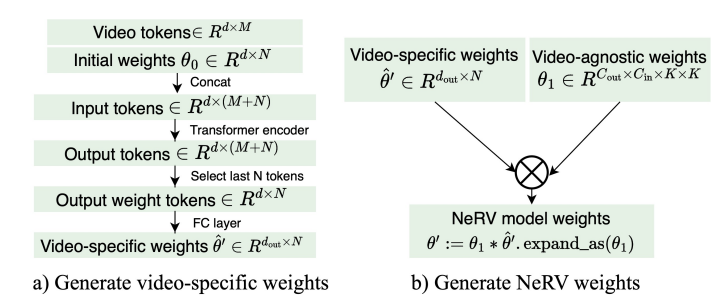
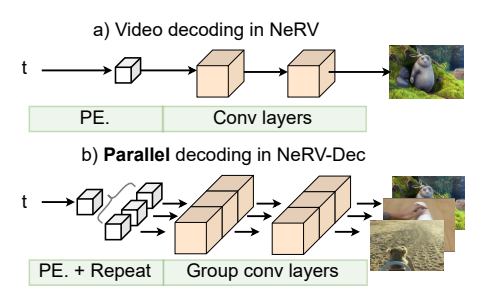


Fig. 4: Left Generate video-specific weights  $\hat{\theta}'$  via the hyper-network. Right Generate NeRV weights  $\theta'$  by element-wise multiplication of  $\hat{\theta}'$  and video-agnostic weights  $\theta_1$ .



**Fig. 5: Parallel video decoding** of NeRV-Dec is achieved using group convolution. NeRV decoding is a special case of NeRV-Dec when the group size is 1. 'PE.' denotes position encoding. 'Repeat' indicates embedding repetition for input expansion.

a convolution layer (with parameters in  $R^{C_{\text{out}} \times C_{\text{in}} \times K \times K}$ ) might be smaller. To compensate, we introduce learnable parameters  $\theta_1 \in R^{C_{\text{out}} \times C_{\text{in}} \times K \times K}$  for each layer, which are shared across all videos and known as video-agnostic parameters. The final weights of the NeRV model, detailed in Fig. 4, are determined by an element-wise multiplication of the video-agnostic weights  $\theta_1$  and the video-specific weights  $\hat{\theta}'$ .

Video Decoding Prelimaries for NeRV. With the final NeRV model weights, we access the video frame using a feedforward operation with the frame index t. Following a common practice in implicit neural representations [6,36], we initially normalize t to the interval [-1, 1], apply positional encoding, and obtain a time embedding vector. This time embedding is used as input to the NeRV model  $f_{\theta}$ , which generates the video frame  $\hat{x}_t$ . The output of the final layer is adjusted by an output bias of 0.5, considering image normalization within the [0, 1] range. In essence, video decoding can be expressed as  $\hat{x}_t = f_{\theta=\theta'}(t)$ , as shown in Fig. 5 (a). Efficient video decoding can be accomplished by running NeRV with a batch size encompassing all frames.

Parallel Decoding for NeRV-Dec. NeRV-Dec enables parallel decoding by running several NeRV models at once, allowing multiple videos to be decoded simultaneously. This process is efficiently executed using group convolution, where each group corresponds to a separate NeRV model, as illustrated in Fig. 5 (b). Note that NeRV decoding is a special case of NeRV-Dec when video number is 1.

Since video decoding is an essential operation in implicit neural representations, this method of parallelization significantly boosts the training speed of NeRV-Enc. Furthermore, it improves the scalability and efficiency of NeRV-Dec when used as a video data loader.

### 3.3 Model Optimization

To optimize NeRV-Enc, our objective is to minimize the reconstruction loss between the ground truth frame  $x_t$  and the reconstructed frame  $\hat{x}_t$ , which is expressed as:

$$\phi^* = \arg\min_{\phi, \theta_0, \theta_1} \sum_{x \in D_{\text{train}}} \sum_t \|f_{\theta = g_{\phi}(x)}(\mathbf{t}) - \mathbf{x}_t\|_2^2$$
 (1)

. Once we have the optimized NeRV-Enc  $\phi^*$ , we evaluate it on the test set  $D_{\text{test}}$ , addressing the two key questions raised in Sec. 1: can NeRV-Enc effectively fit training videos, and can it successfully generalize to test videos.

NeRV-Enc consists of three sets of learnable parameters: those for the hypernetwork  $\phi$ , initial weight tokens  $\theta_0$ , and model-agnostic weights  $\theta_1$ . For optimization, we utilize a training objective based on the mean square error (MSELoss) between the output frame and the ground truth frames.

## 4 Experiment

## 4.1 Datasets and Implementation Details

In our experiments, we utilize three widely-adopted video datasets: Kinetics-400 (K400, our training dataset) [24], Something-Something V2 (SthV2) [18], and UCF101 [46]. Kinetics-400 comprises about 240k training videos and 20k test videos, each lasting 10 seconds, across 400 classes. Due to the extensive size of the full dataset, we may use a subset of K400 for training, consisting of 25 videos per class. For evaluation, we employ the test sets of K400, SthV2 (about 20k motion-centric videos), and UCF101 (about 3.5k human-centric videos). The quality of the reconstructed videos is evaluated using PSNR and SSIM.

The default video size is  $256 \times 256$  with 8 frames. To preprocess the data, we first resize the input video so that its shorter side is 256. We then perform a center crop to obtain a  $256 \times 256$  clip. Subsequently, we uniformly sample 8 frames from the clip and input them to the model. For data tokenization, we divide the videos into  $64 \times 64$  patches. The video model consists of four NeRV blocks, each with upscale factors of 4, 4, 4, and 4, respectively [6]. The convolution layers in these blocks maintain a consistent channel width of 16, except for the first block, where the input channel represents the time embedding dimension, and the last block, where the output channel corresponds to the video channels. The kernel size is 1 for the first convolution layer and 3 for the subsequent ones.

The default transformer hyper-network is composed of 6 encoder layers with a hidden dimension of 720 and a forward dimension of 2800. We employ the

Methods	F	Encoder size	INR size ↓	$\#\hat{\theta}'\downarrow$	Epoch	$\begin{array}{c} \mathrm{GPU} \\ \mathrm{hrs} \downarrow \end{array}$			SNR ↑ SthV2	UCF101	Train		IM ↑ SthV2	UCF101
TransINR [9]	4	48.0M	99k	25k	150	63	23.7	22.1	24.6	22.1	0.659	0.631	0.728	0.622
GINR [27]	4	47.6M	139.4k	25.6k	150	65	24.5	23.2	25.9	23.1	0.685	0.66	0.744	0.66
NeRV-Enc	4	47.6M	85.6k	24.1k	150	9	26.6	26.6	29.4	26	0.756	0.754	0.816	0.752
NeRV-Enc	4	47.6M	85.6k	24.1k	1000	62	27.9	27.5	30.5	27.1	0.794	0.783	0.838	0.783
TransINR [9]	8	48.0M	99k	25k	150	119	22.3	20.3	22.8	20.7	0.626	0.595	0.703	0.591
GINR [27]	8	47.6M	139.4k	25.6k	150	123	23.9	22.8	25.3	22.7	0.671	0.65	0.737	0.651
NeRV-Enc	8	47.6M	85.6k	24.1k	150	11	25.8	25.8	28.5	25.2	0.732	0.727	0.795	0.723
NeRV-Enc	8	47.6M	85.6k	24.1k	1500	110	27.8	27.4	30.3	26.8	0.791	0.78	0.835	0.778
TransINR [9]	16	48.0M	99k	25k	150	234	21.5	18.4	21.1	19.2	0.615	0.555	0.678	0.561
GINR [27]	16	47.6M	139.4k	25.6k	150	242	22.9	21.7	24.2	21.7	0.647	0.624	0.72	0.625
NeRV-Enc	16	47.6M	85.6k	24.1k	150	15	23.6	23.2	25.9	22.9	0.657	0.642	0.731	0.642
${\rm NeRV\text{-}Enc}$	16	47.6M	85.6k	$24.1\mathrm{k}$	2000	200	25.4	24.9	27.7	24.5	0.711	0.693	0.772	0.692

Table 2: NeRV-Enc vs. Pixel-wise INR methods. NeRV-Enc is much faster (up to  $15\times$ ) than pixel-wise methods for training. It also shows better quality in reconstructing videos across datasets, as measured by PSNR and SSIM. 'F' refers to frame number,  $\#\hat{\theta}'$  is the size of video-specific weights. Training time is measured in 'GPU hrs'.

AdamW [33] optimizer with a batch size of 32, an initial learning rate of 1e-4. Our learning rate undergoes a step-wise decay, decreasing by a factor of 0.1 at 90% of the total training steps. Our implementation is built on PyTorch [38]. Model training is conducted using 8 A100 GPUs for all experiments, unless otherwise specified. For video decoding, we test on a machine with 1 A100 GPU and 8 CPUs <sup>4</sup>. Additional implementation details and visualization results are available in the supplementary material.

#### 4.2 Video Encoding

**NeRV-Enc** vs. **Pixel-wise INRs.** We begin by comparing our method to pixel-wise methods TransINR [9] and GINR [26], which also employ hypernetworks for generating implicit representations. However, these methods rely on pixel-wise Implicit Neural Representations (INRs), which exhibit inherent inefficiencies, particularly in large-scale training, as demonstrated in Tab. 2.

Firstly, pixel-wise INRs are notably slower than image-wise INRs, a fact also demonstrated in NeRV [6]. For instance, with the same 150-epoch training, NeRV-Enc outperforms pixel-wise methods, achieving  $\mathbf{7} \times$  faster training for 4 frames,  $\mathbf{10.8} \times$  for 8 frames, and  $\mathbf{15.6} \times$  for 16 frames. Secondly despite having a smaller INR model  $\theta$  and less model-specific weights  $\hat{\theta}'$  (i.e. smaller video size), NeRV-Enc achieves superior video reconstruction quality for both training and testing videos, as measured by PSNR and SSIM metrics. The difference in quality becomes more noticeable when comparing pixel-wise methods to NeRV-Enc with similar training times. In this comparison, NeRV-Enc outperforms them by  $+\mathbf{4.6}$ ,  $+\mathbf{5.0}$ , and  $+\mathbf{4.1}$  PSNR for videos with 8 frames in the K400, SthV2, and UCF101 test sets, respectively. Qualitative results are provided in Fig. 6, comparing NeRV-Enc with pixel-wise methods. These visual comparisons

<sup>&</sup>lt;sup>4</sup> Intel(R) Xeon(R) Platinum 8259CL CPU @ 2.50GHz

c	c	S N		PSN	VR ↑		SSIM ↑ Train K400 SthV2 UCF				
ε ε	S		Train	K400	SthV2	UCF	Train	K400	SthV2	UCF	
			25.8	25.8	28.5	25.2	0.732	0.727	0.795	0.723	
<b>√</b>			27.8	27.4	30.4	26.9	0.791	0.782	0.837 $0.822$ $0.852$	0.781	
	$\checkmark$		26.5	26.7	29.5	26.2	0.756	0.762	0.822	0.759	
		✓	27.8	27.9	30.9	27.4	0.792	0.799	0.852	0.802	
✓	$\checkmark$	$\checkmark$	28.1	28.4	31.6	28.1	0.803	0.808	0.862	0.817	

Table 3: Scale NeRV-Enc by increasing training epochs  $\mathcal{E}$ , hyper-nerwork size  $\mathcal{S}$ , training video number  $\mathcal{N}$ .



**Fig. 6:** Visualizations for INR encoding methods: TransINR [9] (**Top**), GINR [26] (**Middle**), and NeRV-Enc (**Bottom**, ours). Our method excels in reconstructing videos with superior fidelity and fine details. Best viewed digitally and zoomed in.

illustrate that NeRV-Enc excels in capturing videos with superior fidelity and fine details.

Scale NeRV-Enc. We also investigate scaling techniques to further improve the performance of NeRV-Enc: longer training epochs, more training videos, and a larger hyper-network. The results are presented in Tab. 3. It is evident that expanding the training epochs and incorporating more training videos leads to substantial improvements in reconstruction quality, with a notable increase of +2 in PSNR and +0.06 in SSIM for both training and testing videos. Additionally, increasing the size of the hyper-network, together with a larger dropout ratio for transformer layers as well, enhances reconstruction performance. The integration of these three techniques results in our final NeRV-Enc model, leading to +2.6, +3.1, and +2.9 PSNR improvements for three test sets. We find that NeRV-Enc's reconstruction performance improves with increased computational resources and provide more ablation results in the appendix.

NeRV-Enc vs. NeRV. Using the finalized NeRV-Enc, we compare it with the NeRV baseline [6] which uses gradient-based optimization for model fitting and video encoding. The results, depicted in Fig. 7, highlight the effective generalization of NeRV-Enc across various video datasets, including K400, SthV2 and UCF101. Significantly, NeRV-Enc demonstrates a remarkable encoding acceleration, being  $\mathbf{10^4} \times$  times faster than the NeRV baseline, yet maintaining comparable output quality, as measured by PSNR and SSIM metrics. It's noteworthy that NeRV-Enc enables real-time video encoding, positioning implicit video representation as a viable and efficient option for video codec.

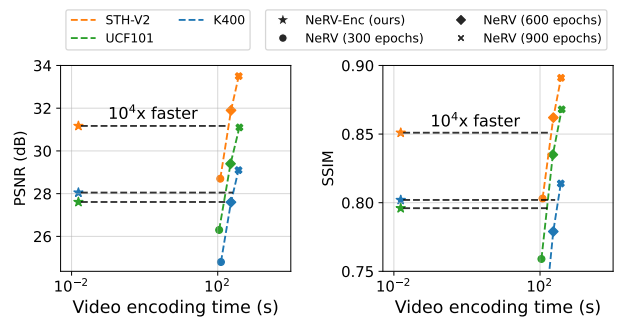


Fig. 7: Encoding speed. NeRV-Enc (ours) is  $10^4 \times$  faster than NeRV [6] baseline (using gradient-based optimization) across multiple datasets.



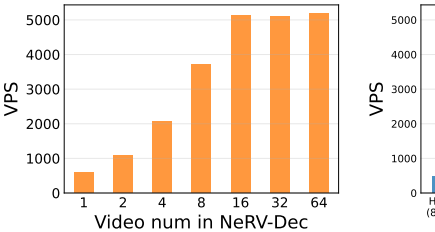
Fig. 8: Top: input videos with various degradations from test set. Bottom: output videos of NeRV-Enc. *Left*: downsampled; *Middle*: blurred; *Right*: mask.

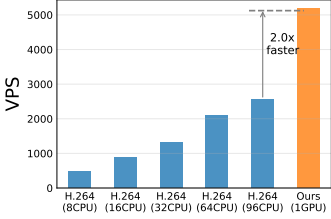
Methods	Layer $1/2/3/4$ params	TotalParam	Train	K400	SthV2	UCF101
Layer-uniform [9] Layer-specific [27]	$\begin{array}{c} 4.1 k\_9.2 k\_9.2 k\_6.9 k \\ 0\_36.9 k\_0\_0 \end{array}$	$\begin{array}{c} 29.4 \mathrm{k} \\ 36.9 \mathrm{k} \end{array}$	$22.1 \\ 25.5$	$21.5 \\ 25.4$	24.1 28.1	$21.6 \\ 24.8$
Layer-adaptive (ours)	0_18.4k_0_0 1.1k_18.4k_4.6k_0	18.4k <b>24.1k</b>	25.1 <b>25.8</b>	25.0 <b>25.8</b>	27.7 <b>28.5</b>	24.4 25.2
	2.4k_18.4k_4.6k_0 1.1k_18.4k_9.2k_0 1.1k_18.4k_4.6k_0.1k	$25.4 \mathrm{k} \ 28.7 \mathrm{k} \ 24.2 \mathrm{k}$	25.5 25.8 25.7	25.4 25.8 25.6	28.2 28.5 28.3	25.0 <b>25.3</b> 25.1

Table 4: Ablation Study on layer-daptive modulation. We compare uniform tokens (TransINR [9]), layer-specific tokens (GINR [27]), and our layer-adaptive tokens. Our approach surpasses the layer-specific method in reconstruction performance (PSNR  $\uparrow$ ) and achieves a 50% reduction in video size (total parameters  $\downarrow$ ).

NeRV-Enc for Video Restoration. Like prior methods that use implicit representations for videos, we found that NeRV-Enc is also effective for video restoration tasks. Our findings, detailed in Fig. 8, cover three types of video degradation: downsampling, blurring, and masking of input videos. We observed that these degradations in pixel space are effectively restored in implicit space. While our primary focus in this paper is on fast encoding and decoding, we have included quantitative results in the appendix for further reference.

Ablation for Layer-adaptive Modulation. The ablation study on layer-wise modulation is presented in Tab. 4, demonstrating that even with reduced parameters in Layer 2 (see row 3), we can achieve results on par with the layer-specific approach (see row 2). Moreover, we incrementally increase parameters in other layers (rows 4 to 7) until no additional improvements were observed. In examin-





**Fig. 9: Left:** NeRV-Dec's decoding speed scales efficiently with increasing video numbers. Note NeRV decoding is a special case of NeRV-Dec when video number is 1 (the leftmost bar). **Right:** NeRV-Dec is  $2 \times$  faster than H.264 with **96** CPUs.

ing the distribution of weight tokens, we evaluate uniform tokens (TransINR [9]), layer-specific tokens (GINR [27]), and our proposed layer-adaptive weight tokens, which use  $29.4 \, \mathrm{K}$ ,  $36.9 \, \mathrm{K}$ , and  $24.1 \, \mathrm{K}$  video-specific weights, respectively. The results indicate that our approach not only achieves better reconstruction quality but also does so with fewer video-specific parameters, contributing to reduced video size and enhanced compression efficiency. Note that our layer-adaptive modulation (highlighted in the gray row) not only surpasses the performance of the layer-specific method but also achieves a 50% reduction in the total number of parameters (video size).

#### 4.3 Video Decoding

Parallelization. NeRV-Dec improves upon NeRV by using multiple stacked models to decode several videos at once. Its efficiency comes from a shared time embedding layer and a group convolution process that can be parallelized. We evaluate this parallelization by varying the number of videos for decoding. NeRV decoding is a specific case of NeRV-Dec when decoding video number is 1. As shown in Fig. 9 (Left), there is a near-linear speedup in decoding as video batch size increases from 1 to 16. Beyond a batch size of 16, decoding speed plateaus around 5200 videos per second, maximizing GPU usage. Video decoding (data loading) is crucial as videos are decoded repeatedly, essential for playback, streaming, and research. Preview of multiple videos is also common for video platforms. Typically, videos are divided into clips or picture groups for storage. Our parallel decoding significantly boosts video loading efficiency.

Comparison with H.264. NeRV-Dec outperforms a traditional data loader using the H.264 codec (485 videos per second for 8 CPUs), achieving a  $11\times$  increase in loading speed. To further understand the decoding performance of H.264, we explore various ways for its speed improvement. Surprisingly, transitioning from CPU to GPU as the decoding device does not yield speed gains, except for larger videos. Consequently, we increase the number of CPUs and data loader workers, presenting the results in Fig. 9 (Right). The results show that while augmenting the CPU count enhances video loading speed, the improvements diminish, especially beyond 16 CPUs. It's worth noting that even with 96 CPUs, H.264 is still

	DAM AV1			H.264		NeRV-Dec (ours) 8 bits 7 bits 6 bits 5 bits 4 bits				
	n AM	CRF 60	CRF 35	$\mathrm{CRF}\ 40$	$\mathrm{CRF}\ 45$	8 bits	7 bits	6 bits	5 bits	4 bits
Size ↓	1.15MB	21.9KB	20.4KB	13.1KB	8.7KB	23.7KB	20.7KB	17.7KB	14.7KB	11.6KB
PSNR ↑	-	32.4	32.8	30.0	27.3	28.4	28.3	28.1	27.5	25.6
SSIM $\uparrow$	-	0.910	0.912	0.860	0.788	0.808	0.807	0.802	0.784	0.712
$VPS \uparrow$	2031	313	447	460	485			5175		

**Table 5: Detailed comparison.** NeRV-Dec reduces video size by  $65 \times$  via weight quantization, while being  $2.5 \times$  faster than loading pre-decoded videos from RAM. Although AV1 and H.264 provide better compression (smaller video size) and video quality (higher PSNR and SSIM), NeRV-Dec decodes videos much faster (higher VPS).

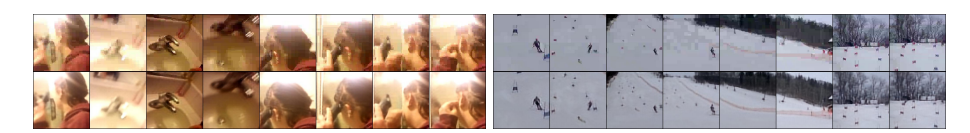


Fig. 10: Visual comparison: H.264 (Top) vs. NeRV-Dec (Bottom) at similar PSNR. H.264 exhibits noticeable blocking artifacts, whereas NeRV-Dec provides a more visually appealing result. Best viewed digitally and zoomed in.

 $2\times$  slower than our NeRV-Dec. Given that powerful chips like GPUs are already preferred for deep learning practitioners, the video loading advantages of NeRV-Dec can be leveraged without the need for additional hardware or specialized design and optimization.

**Detailed Comparisons.** Besides the video decoding speed, we conduct a comprehensive assessment of NeRV-Dec, examining video reconstruction quality and compression performance. Our method undergoes comparisons against various video representations, including traditional codecs like H.264 and AV1, as well as RAM reading (load pre-decoded videos from RAM) for efficient data loading. Detailed results are presented in Tab. 5.

Video Compression. To compress the video size in NeRV-Dec, we implement quantization to the video-specific weights  $(\hat{\theta}')$  and employ Huffman encoding. These techniques substantially decreases disk storage requirements while maintaining video quality. It retains 99% of the PSNR and SSIM values of the original model using just 6 bits per parameter. With a reduced video size (65× smaller), NeRV-Dec even surpasses loading videos from RAM, achieving a 2.5× faster speed with GPU assistance. As deep learning platforms commonly utilize powerful hardware like GPUs for computation, the fast and simple video loading provided by NeRV-Dec can significantly enhance video research and alleviate data loading bottlenecks.

Comparison with Traditional Codecs. While the compression ratio of our method is slightly lower than that of conventional codecs such as  $\rm H.264$  and  $\rm AV1$ , our method is  $\rm 11\times$  faster in video decoding and can be easily implemented on most devices without any specific design or optimization. As outlined in Tab. 3, enhancing the scale of NeRV-Enc's training by employing additional

		P	SNR ↑		SSIM ↑  Train K400 SthV2 UCF101			
INR	Train	K400	SthV2	UCF101	Train	K400	SthV2	UCF101
NeRV	25.8	25.8	28.5	25.2 22.6	0.732	0.727	0.795	0.723
HNeRV	23.1	22.9	25.1	22.6	0.647	0.644	0.727	0.642

Table 6: NeRV-Enc results for NeRV and hybrid INR (HNeRV).

resources (like more videos for training, extended training epoches, or a larger hyper-network) could yield further improvements and lead to better compression performance. Beyond just numerical comparisons, we provide visual comparisons between H.264 and NeRV-Dec at an equivalent PSNR of 28.1, as shown in Fig. 10. These visual examples clearly demonstrate the blocking artifacts present in H.264, emphasizing the superior visual quality offered by NeRV-Dec. This This advantage highlights the potential preference for NeRV-Dec in scenarios where visual quality is a priority.

#### 4.4 Limitations and Future Works

 $Hybrid\ INRs$  enhance the NeRV framework by utilizing inputs that are either content-adaptive embeddings or learnable 2D/3D grids. These enhancements allow for superior performance in tasks like video compression or interpolation compared to the original NeRV. We extend NeRV-Enc to also produce these video-specific embeddings or learnable grid features, which then serve as inputs for NeRV. We show results in Tab. 6 and NeRV-Enc is adaptable to diverse INR methods. While NeRV-Enc shows promise in facilitating hybrid INRs, further investigation is required to achieve better results. The hybrid INR approach (HNeRV), which involves learning both input embedding and decoder weights, necessitates a more complex design.

NeRV-Enc does not yet match the performance of established video codecs such as H.264 in video compression. Closing this performance gap is another focus for our future work. Meanwhile, further exploration of reconstruction loss and restoration tasks holds promise to produce visually-appealing results.

#### 5 Conclusion

In this paper, we introduce NeRV-Enc, a hyper-network that improve encoding speed by generating weights for the NeRV model. Our findings reveal that NeRV-Enc significantly accelerates the encoding process, achieving a remarkable speed-up of  $10^4$  times compared to the traditional training of NeRV using gradient-based optimization. Additionally, we present NeRV-Dec, a parallel video decoder that surpasses traditional codecs in speed by  $11\times$ , and outperforms the speed of loading pre-decoded videos from RAM by  $2.5\times$ .

#### References

- Agustsson, E., Minnen, D., Johnston, N., Balle, J., Hwang, S.J., Toderici, G.: Scale-space flow for end-to-end optimized video compression. In: CVPR (June 2020) 4
- 2. Anokhin, I., Demochkin, K., Khakhulin, T., Sterkin, G., Lempitsky, V., Korzhenkov, D.: Image generators with conditionally-independent pixel synthesis. In: CVPR. pp. 14278–14287 (2021) 3
- Bross, B., Wang, Y.K., Ye, Y., Liu, S., Chen, J., Sullivan, G.J., Ohm, J.R.: Overview of the versatile video coding (vvc) standard and its applications. IEEE Transactions on Circuits and Systems for Video Technology 31(10), 3736–3764 (2021) 4
- 4. Carion, N., Massa, F., Synnaeve, G., Usunier, N., Kirillov, A., Zagoruyko, S.: Endto-end object detection with transformers. In: ECCV. Springer (2020) 2
- 5. Chen, H., Gwilliam, M., Lim, S.N., Shrivastava, A.: HNeRV: Neural representations for videos. In: CVPR (2023) 1, 3, 6
- Chen, H., He, B., Wang, H., Ren, Y., Lim, S.N., Shrivastava, A.: NeRV: Neural representations for videos. In: NeurIPS (2021) 1, 2, 3, 4, 6, 7, 8, 9, 10, 11
- 7. Chen, H., Matthew, A.G., He, B., Lim, S.N., Shrivastava, A.: CNeRV: Content-adaptive neural representation for visual data. In: BMVC (2022) 1, 3
- 8. Chen, Y., Liu, S., Wang, X.: Learning continuous image representation with local implicit image function. In: CVPR. pp. 8628–8638 (2021) 3
- Chen, Y., Wang, X.: Transformers as meta-learners for implicit neural representations. In: European Conference on Computer Vision (2022) 4, 6, 9, 10, 11, 12, 2
- 10. Chen, Y., Dai, X., Liu, M., Chen, D., Yuan, L., Liu, Z.: Dynamic convolution: Attention over convolution kernels. In: CVPR. pp. 11030–11039 (2020) 4
- Chen, Y., Murherjee, D., Han, J., Grange, A., Xu, Y., Liu, Z., Parker, S., Chen, C., Su, H., Joshi, U., et al.: An overview of core coding tools in the av1 video codec. In: 2018 Picture Coding Symposium (PCS). pp. 41–45. IEEE (2018) 4
- 12. Chen, Z., Chen, Y., Liu, J., Xu, X., Goel, V., Wang, Z., Shi, H., Wang, X.: Videoinr: Learning video implicit neural representation for continuous space-time super-resolution. CVPR (2022) 1
- 13. Chen, Z., Zhang, H.: Learning implicit fields for generative shape modeling. In: CVPR (June 2019)  $\frac{3}{2}$
- Djelouah, A., Campos, J., Schaub-Meyer, S., Schroers, C.: Neural inter-frame compression for video coding. In: ICCV (2019) 4
- Dosovitskiy, A., Beyer, L., Kolesnikov, A., Weissenborn, D., Zhai, X., Unterthiner, T., Dehghani, M., Minderer, M., Heigold, G., Gelly, S., Uszkoreit, J., Houlsby, N.: An image is worth 16x16 words: Transformers for image recognition at scale. In: ICLR (2021), https://openreview.net/forum?id=YicbFdNTTy 2
- 16. Dupont, E., Goliński, A., Alizadeh, M., Teh, Y.W., Doucet, A.: Coin: Compression with implicit neural representations. In: ICLR workshop (2021) 3
- 17. Feichtenhofer, C., Li, Y., He, K., et al.: Masked autoencoders as spatiotemporal learners. Advances in neural information processing systems **35**, 35946–35958 (2022) 2
- 18. Goyal, R., Kahou, S.E., Michalski, V., Materzynska, J., Westphal, S., Kim, H., Haenel, V., Fründ, I., Yianilos, P., Mueller-Freitag, M., Hoppe, F., Thurau, C., Bax, I., Memisevic, R.: The "something something" video database for learning and evaluating visual common sense. In: ICCV (2017) 8
- 19. Ha, D., Dai, A.M., Le, Q.V.: Hypernetworks. In: ICLR (2017) 3

- Habibian, A., Rozendaal, T.v., Tomczak, J.M., Cohen, T.S.: Video compression with rate-distortion autoencoders. In: ICCV (2019) 4
- He, B., Yang, X., Wang, H., Wu, Z., Chen, H., Huang, S., Ren, Y., Lim, S.N., Shrivastava, A.: Towards scalable neural representation for diverse videos. In: CVPR (2023) 1, 3
- 22. He, K., Chen, X., Xie, S., Li, Y., Dollár, P., Girshick, R.: Masked autoencoders are scalable vision learners. CVPR (2022) 2
- Karras, T., Aittala, M., Laine, S., Härkönen, E., Hellsten, J., Lehtinen, J., Aila, T.: Alias-free generative adversarial networks. arXiv preprint arXiv:2106.12423 (2021)
- Kay, W., Carreira, J., Simonyan, K., Zhang, B., Hillier, C., Vijayanarasimhan, S., Viola, F., Green, T., Back, T., Natsev, P., et al.: The kinetics human action video dataset. arXiv preprint arXiv:1705.06950 (2017) 8
- Khani, M., Sivaraman, V., Alizadeh, M.: Efficient video compression via contentadaptive super-resolution. arXiv preprint arXiv:2104.02322 (2021) 4
- 26. Kim, C., Lee, D., Kim, S., Cho, M., Han, W.S.: Generalizable implicit neural representations via instance pattern composers. CVPR (2023) 4, 6, 9, 10
- Kim, S., Yu, S., Lee, J., Shin, J.: Scalable neural video representations with learnable positional features. NeurIPS (2022) 1, 6, 9, 11, 12, 2
- Le Gall, D.: Mpeg: A video compression standard for multimedia applications. Commun. ACM (1991) 4
- 29. Li, Z., Wang, M., Pi, H., Xu, K., Mei, J., Liu, Y.: E-nerv: Expedite neural video representation with disentangled spatial-temporal context. ECCV (2022) 1, 3
- Liu, H., Chen, T., Lu, M., Shen, Q., Ma, Z.: Neural video compression using spatiotemporal priors. arXiv preprint arXiv:1902.07383 (2019) 4
- 31. Liu, J., Wang, S., Ma, W.C., Shah, M., Hu, R., Dhawan, P., Urtasun, R.: Conditional entropy coding for efficient video compression. In: ECCV (2020) 4
- 32. Liu, Z., Lin, Y., Cao, Y., Hu, H., Wei, Y., Zhang, Z., Lin, S., Guo, B.: Swin transformer: Hierarchical vision transformer using shifted windows. ICCV (2021)
- 33. Loshchilov, I., Hutter, F.: Decoupled weight decay regularization. arXiv preprint arXiv:1711.05101 (2017) 9
- 34. Mehta, I., Gharbi, M., Barnes, C., Shechtman, E., Ramamoorthi, R., Chandraker, M.: Modulated periodic activations for generalizable local functional representations. In: ICCV. pp. 14214–14223 (2021) 3
- 35. Mescheder, L., Oechsle, M., Niemeyer, M., Nowozin, S., Geiger, A.: Occupancy networks: Learning 3d reconstruction in function space. In: CVPR (June 2019) 4
- 36. Mildenhall, B., Srinivasan, P.P., Tancik, M., Barron, J.T., Ramamoorthi, R., Ng, R.: Nerf: Representing scenes as neural radiance fields for view synthesis. In: ECCV. pp. 405–421. Springer (2020) 3, 7
- 37. Park, J.J., Florence, P., Straub, J., Newcombe, R., Lovegrove, S.: Deepsdf: Learning continuous signed distance functions for shape representation. In: CVPR (June 2019) 3, 4
- 38. Paszke, A., Gross, S., Massa, F., Lerer, A., Bradbury, J., Chanan, G., Killeen, T., Lin, Z., Gimelshein, N., Antiga, L., Desmaison, A., Kopf, A., Yang, E., DeVito, Z., Raison, M., Tejani, A., Chilamkurthy, S., Steiner, B., Fang, L., Bai, J., Chintala, S.: Pytorch: An imperative style, high-performance deep learning library. In: NeurIPS (2019) 9
- 39. Rippel, O., Anderson, A.G., Tatwawadi, K., Nair, S., Lytle, C., Bourdev, L.: Elf-vc: Efficient learned flexible-rate video coding. In: ICCV (2021) 4

- 40. Rippel, O., Nair, S., Lew, C., Branson, S., Anderson, A.G., Bourdev, L.: Learned video compression. In: ICCV (2019) 4
- 41. Schwarz, K., Liao, Y., Niemeyer, M., Geiger, A.: Graf: Generative radiance fields for 3d-aware image synthesis. In: NeurIPS (2020) 3
- 42. Sitzmann, V., Martel, J.N.P., Bergman, A.W., Lindell, D.B., Wetzstein, G.: Implicit neural representations with periodic activation functions. In: NeurIPS (2020)
- 43. Sitzmann, V., Martel, J.N., Bergman, A.W., Lindell, D.B., Wetzstein, G.: Implicit neural representations with periodic activation functions. In: NeurIPS (2020) 4
- 44. Sitzmann, V., Zollhöfer, M., Wetzstein, G.: Scene representation networks: Continuous 3d-structure-aware neural scene representations. In: NeurIPS (2019) 4
- Skorokhodov, I., Ignatyev, S., Elhoseiny, M.: Adversarial generation of continuous images. In: CVPR. pp. 10753–10764 (2021) 3
- 46. Soomro, K., Za4mir, A.R., Shah, M.: Ucf101: A dataset of 101 human actions classes from videos in the wild. arXiv preprint arXiv:1212.0402 (2012) 8
- 47. Sullivan, G.J., Ohm, J.R., Han, W.J., Wiegand, T.: Overview of the high efficiency video coding (hevc) standard. IEEE Transactions on Circuits and Systems for Video Technology (2012) 4
- 48. Tancik, M., Srinivasan, P.P., Mildenhall, B., Fridovich-Keil, S., Raghavan, N., Singhal, U., Ramamoorthi, R., Barron, J.T., Ng, R.: Fourier features let networks learn high frequency functions in low dimensional domains. In: NeurIPS (2020) 3
- Touvron, H., Cord, M., Douze, M., Massa, F., Sablayrolles, A., Jégou, H.: Training data-efficient image transformers & distillation through attention. In: ICML. pp. 10347–10357. PMLR (2021) 2
- 50. Wiegand, T., Sullivan, G.J., Bjontegaard, G., Luthra, A.: Overview of the h. 264/avc video coding standard. IEEE Transactions on circuits and systems for video technology (2003) 4
- 51. Wu, C.Y., Girshick, R., He, K., Feichtenhofer, C., Krahenbuhl, P.: A multigrid method for efficiently training video models. In: CVPR. pp. 153–162 (2020) 2
- 52. Wu, C.Y., Singhal, N., Krahenbuhl, P.: Video compression through image interpolation. In: ECCV (2018) 4
- 53. Yang, B., Bender, G., Le, Q.V., Ngiam, J.: Condconv: Conditionally parameterized convolutions for efficient inference. NeurIPS **32** (2019) **4**

## A Implementation Details

#### A.1 Pseudocode of NeRV-Enc and NeRV-Dec

We firstly provide pseudocode for NeRV-Enc and NeRV-Dec in Algorithm 1.

## Algorithm 1 Pseudocode in a PyTorch style.

```
######### 1) Video encoding: NeRV-Enc ##########
# Input: video x, initial weights 	heta_0
# Output: video-specific weights \hat{	heta}'
# Video tokenization
                                                                                                 # d \times M
x = FC_1(x.tokennize())
# Concat video patches and initial weights as input
x = x.concat(\theta_0)
                                                                                            # d \times (M+N)
# Hypernetwork g_\phi output video-specific weights \hat{	heta}'
\hat{\theta}' = g_{\phi}.forward(x)[-N:].
                                                                                                 # d \times N
\hat{\theta}' = FC_2(\hat{\theta}')
                                                                                              # C_{\text{out}} \times N
########## 2) Video decoding: NeRV-Dec ##########
\hat{\theta}' = \hat{\theta}'.expand_as(\theta_1)
                                                                             # broadcast into needed shape
\theta' = \theta_1 * \hat{\theta}'
                                                                       # Cout \times Cin \times K \times K
# Initial NeRV model f_{	heta} with generated weights
f_{-}\theta.reset_parameter(\theta')
# Input frame index t, and output video frame \hat{x}_{\mathrm{t}}
\hat{x}_t = f_\theta. \text{forward(t)}
# Compute loss and backward gradients
loss = MSELoss(\hat{x}_t, x_t)
loss.backward()
# update all learnable parameters
update([\phi, \theta_0, \theta_1])
```

FC: fully connected layer; MSELoss: mean square error loss.

#### A.2 Scaling the training of NeRV-Enc

We explore factors such as the number of training videos, training epochs, encoder size, and weight token distributions, as outlined in Tab. 7. Generally, NeRV-Enc's reconstruction performance improves with increased computational resources, although the gains tend to plateau as training duration becomes adequate. Higher dropout ratios are essential for achieving improved generalization in longer training epochs or with larger hyper-networks. These ablations underscore that the reconstruction quality of NeRV-Enc can be significantly enhanced by scaling the training with additional resources, including more training videos, longer training epochs, and larger hyper-networks.

		$P_{s}^{s}$	SNR ↑		SSIM $\uparrow$						
	Train	K400	SthV2	UCF101	Train	K400	SthV2	UCF101			
Epocl	Epoch ablation										
150	25.8	25.8	28.5	25.2	0.732	0.727	0.795	0.723			
300	26.8	26.7	29.5	26.2	0.763	0.757	0.819	0.757			
600	27.2	27.1	30	26.6	0.774	0.768	0.827	0.766			
1200	27.6	27.3	30.2	26.7	0.787	0.776	0.832	0.774			
1800	27.8	27.4	30.4	26.9	0.791	0.782	0.837	0.781			
Enco	Encoder size ablation										
$47.6\mathrm{M}$	25.8	25.8	28.5	25.2	0.732	0.727	0.795	0.723			
125M	26.4	26.2	28.9	25.6	0.751	0.743	0.806	0.737			
251M	26.5	26.7	29.5	26.2	0.756	0.762	0.822	0.759			
404M	26.5	26.5	29.3	25.9	0.753	0.755	0.816	0.751			
Video	num	ber ab	lation								
10k	25.8	25.8	28.5	25.2	0.732	0.727	0.795	0.723			
20k	26.7	26.6	29.4	26	0.757	0.752	0.814	0.751			
40k	27	26.9	29.7	26.4	0.764	0.761	0.821	0.762			
80k	27.6	27.7	30.6	27.2	0.791	0.791	0.845	0.794			
240k	27.8	27.9	30.9	27.4	0.792	0.799	0.852	0.802			

Table 7: NeRV-Enc ablations. For ablation of weight tokens, we compare uniform tokens (TransINR [9]), layer-specific tokens (GINR [27] at the 2nd layer), and our proposed layer-adaptive weight tokens. Please refer to the main paper for their distinction.

#### A.3 NeRV-Enc for video restoration tasks.

Our NeRV-Enc framework is versatile across various downstream tasks, and shows robust restoration quality for various degradations. Results in ?? and Tab. 8 demonstrate that the reconstruction quality for downsampled, blurred, and masked input videos is comparable to that achieved through conventional video regression. This underscores the framework's effectiveness in restoring common pixel degradations within the implicit space.

Input		Inpu	t PSNI	₹	Output PSNR				
degradation	Train	k400	sth-v2	ucf101	Train	k400	sth-v2	ucf101	
Downsample	20.1	20.3	22.9	19.5	24.5	24.3	26.8	23.9	
Gaussian blur	23.1	23.3	26.0	22.3	24.8	24.7	27.3	24.0	
Inpainting	19.0	18.6	18.1	18.4	25.5	25.2	27.9	24.7	
No	-	-	-	-	25.8	25.8	28.5	25.2	

Table 8: Results for downstream tasks with NeRV-Enc.

#### A.4 Weight quantization for efficient storage.

In this quantization procedure, each element of a vector  $\mu$  is mapped to the nearest integer using the linear transformation defined by the formula:

$$\mu_i = \text{Round}\left(\frac{\mu_i - \mu_{\min}}{\text{scale}}\right) * \text{scale} + \mu_{\min}, \text{ where}$$

$$\text{scale} = \frac{\mu_{\max} - \mu_{\min}}{2^b - 1},$$
(2)

Here,  $\mu_i$  represents a vector element, Round is a rounding function, b is the quantization bit length,  $\mu_{\text{max}}$  and  $\mu_{\text{min}}$  are the maximum and minimum values of vector  $\mu$ , and 'scale' is the scaling factor. Additionally, we use Huffman encoding to further reduce the disk storage.

Results for Model Quantization We extend our analysis on model quantization in Tab. 9, assessing performance on three datasets: K400, Something-V2, and UCF-101.

Bits	K400	PSNR STH-V2	↑ UCF101	K400	SSIM STH-V2	↑ 2 UCF101
32	28.4	31.6	28.1	0.808	0.862	0.817
8	28.4	31.5	28.1	0.808	0.861	0.816
7	28.3	31.5	28	0.807	0.86	0.815
6	28.1	31.2	27.9	0.802	0.855	0.811
5	27.5	30.2	27.3	0.784	0.836	0.794
4	25.6	27.7	25.6	0.712	0.759	0.725

Table 9: Ablation study on model quantization.

#### A.5 Implementation details

Video Encoding. We firstly provide training details of NeRV-Enc below.

- NeRV-Enc:
  - $\bullet$  Video: 8 frames, frame stride evenly sample from the whole video,  $256 \times 256$  resolution.
  - Batch size: 32
  - Patch size: 64
  - Position embedding dimension for NeRV: 16
  - Activation layer in NeRV: GeLU
  - Kernel size for convolution layers in NeRV: 1, 3, 3, 3
  - Upscale factor for NeRV blocks: 4, 4, 4, 4
  - Token number for NeRV layers: 4, 128, 64, 0
  - Token dimensions for NeRV layers: 256, 144, 288, 0

- Model dimension and feed-forward dimension for transformer encoder layers: 720 and 2800 for NeRV-Enc of 47.6M, 1600 and 6400 for NeRV-Enc of larger NeRV-Enc (251M)
- Dropout ratio in transformer encoder layers: 0 for default training, 0.15 for larger NeRV-Enc and long training
- Optimizer: AdamWLearning rate: 0.0001

Video Decoding. To assess the decoding speed of NeRV-Dec, H.264, RAM, and AV1, we employ a PyTorch dataloader to facilitate parallel decoding. We initially stack the NeRV model weights before inputting them into NeRV-Dec. Regarding video compression, we utilize the 'torchvision.io.write\_video' function to store videos, applying various CRF (Constant Rate Factor) settings. For video loading, we experiment with two backends: 'decord' and 'torchvision.io.read\_video', selecting the one that offers superior performance for H.264 and AV1.

## B Hurdles When Converting MLP to CNN

We address the difficulties encountered when converting MLP to CNN for NeRV-Enc, as detailed in Tab. 10. The final model weights  $\theta'$  result from the elementwise multiplication of  $\hat{\theta}' \in \mathbb{R}^{d_{\text{out}} \times N}$  and video-agnostic weights  $\theta_1 \in \mathbb{R}^{C_{\text{out}} \times C_{\text{in}} \times K \times K}$ , as illustrated in Figs. 2 and 4 of the main paper. This is expressed as

$$\theta' := \theta_1 * \hat{\theta}'. \text{expand}_{as}(\theta_1), \tag{3}$$

and is followed by L2 normalization. a) Omitting the *final normalization* leads to a significant performance drop, from 25.8 to 22.9 for the K400 test PSNR. b) Convolution initialization of  $\theta_1$  is crucial, as it increases the test PSNR by approximately 1.8. c) The choice of expansion dimension when expanding  $\hat{\theta}'$  to match  $\theta_1$ 's shape is pivotal. Expanding along dimension -2 (the default choice) produces the best results compared to dimensions -1 and -3.

Method	Train	K400	SthV2	UCF101
NeRV-Enc	25.8	25.8	28.5	25.2
		22.9	25.7	22.9
w/o ConvInit $\theta_1$	24.1	24	26.7	23.5
Expand $\hat{\theta}'$ at dim = -1	24.6	24.3	26.9	23.8
Expand $\hat{\theta}'$ at dim = -3	24.2	23.9	26.5	23.4

**Table 10:** Challenges in converting MLPs to ConvNets, showcasing normalized final weights  $\theta'$ , convolution initialization of  $\theta_1$ , and expansion dimension for  $\hat{\theta}'$ . PSNR $\uparrow$  showed, the higher the better.